

MARVEL: optical fibre link

Gerardo Avila^{*a}, Gert Raskin^b, Christian Schwab^c, Jacob Pember^{b,c}, Bart Vandenbussche^b, Hans Van Winckel^b, Carlos Guirao^e, Roman Guemperlein^a, Julian Stürmer^d

^aBaader Planetarium, Zur Sternwarte 4, 82291, Mammendorf, Germany

^bInstitute of Astronomy, KU Leuven, 3001 Leuven, Belgium

^cDepartment of Physics and Astronomy, Macquarie University, Sydney, Australia

^dLandessternwarte Königstuhl, Heidelberg, Germany

^eEuropean Southern Observatory, Germany

ABSTRACT

MARVEL is a novel facility, consisting of an array of four robotic 80-cm telescopes and one high-resolution Échelle spectrograph. It targets extreme precision radial velocity observations for measuring the mass of exoplanets. The MARVEL spectrograph will be linked to the telescopes through a set of optical fibres. This fibre link consists of a combination of circular and octagonal fibres in an effort to maximize the photometric scrambling gain and hence, the illumination stability of the spectrograph. In this contribution, we present the design of the fibre link, as well as the results of a test campaign that evaluated the relevant characteristics of several circular and octagonal fibres. Based on this, we also report on the expected performances of the MARVEL fibre link.

Keywords: Optical fibres, astronomical instrumentation, photometric scrambling, modal scrambling

1. INTRODUCTION

MARVEL is dedicated to extreme precision radial velocity spectroscopy using an array of four robotic telescopes feeding one spectrograph. It will enable simultaneous RV measurements of up to four bright targets distributed over the sky. Figure 1 shows the conceptual layout of the MARVEL facility. It consists of four commercial-off-the-shelf (COTS) telescopes with a diameter of 80 cm operating at $f/10$. Each telescope will be equipped with a fibre adapter front end and coupled through an optical fibre to the common high-resolution Échelle spectrograph. This instrument will have a spectral resolution $R = \lambda/\Delta\lambda$ of at least 90 000 and cover a very large wavelength range: 390 to 920 nm. The four stellar spectra are interlaced with a fifth spectrum from a wavelength calibration source that is used to track the instrumental drift during each exposure, this way increasing the RV accuracy. The MARVEL detector is a back-illuminated STA1600 CCD with $10.3k \times 10.3k$ 9- μ m pixels (95 \times 95 mm image area). A detailed description of the project is found in [1].

The spectrograph is fed by five octagonal-core fibres (4 science fibres + 1 simultaneous wavelength calibration fibre) with a width of 40 μ m. At the spectrograph entrance, the focal ratio of the beam exiting the fibres is converted from $f/4$ to $f/8$ by a set of focal ratio adaption optics, consisting of one doublet and one triplet lens. To increase throughput, the five fibres are aligned and cemented on the flat entrance surface of the first lens. Outside the vacuum vessel, the four octagonal science fibres are butt-to-butt coupled and accurately aligned to four circular fibres that run to the four telescopes. Combining circular and octagonal fibres breaks the circular symmetry of the former and

*avila.soberanes@gmail.com

increases the overall scrambling performance of the fibre link without the throughput penalty of adding an optical double scrambler. This technique has been used successfully in CARMENES [2] [3]. It results in improved image and pupil stability in the spectrograph with respect to a single fibre, and hence, increased RV precision. The 40 μm fibre diameter in the focal plane of each telescope corresponds to a comfortably large sky aperture of 2.3 arcsec without having to resort to image or pupil slicing.

2. MARVEL FIBRE LINK

A summary of the specifications of the MARVEL fibre link is shown in Table 1. The plate scale generated by the telescope at $f/10$ is 38.79 $\mu\text{m}/\text{arcsec}$ and 17.45 $\mu\text{m}/\text{arcsec}$ at $f/4.5$. Therefore the fibre core sees 2.29 arcsec on the sky.

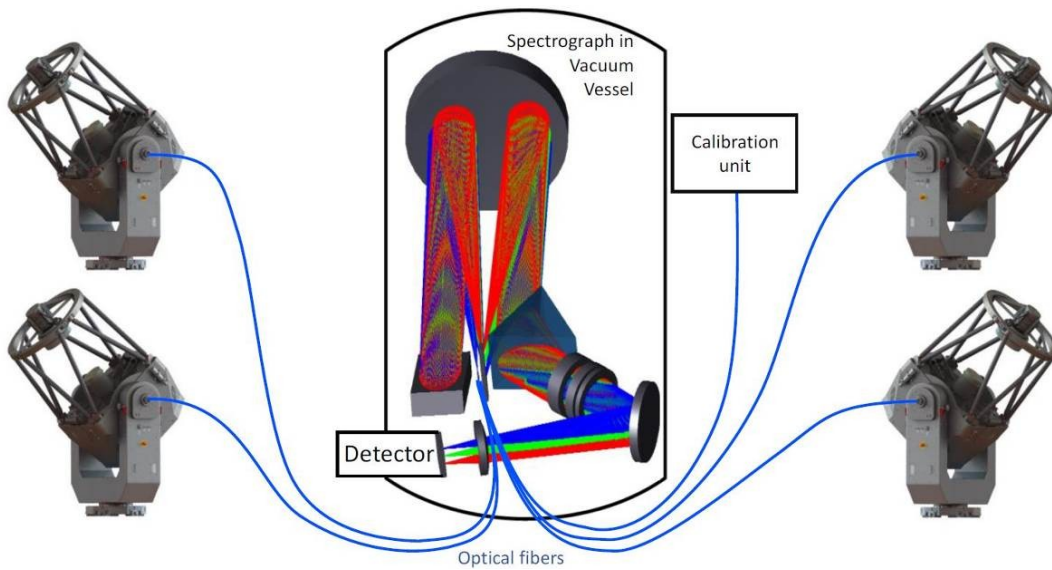


Figure 1. Conceptual diagram of the Marvel project.

One proposed optical coupling between the telescope and the fibre is shown in Figure 2. The $f/10$ telescope beam is reduced to $f/4.5$ by means of two doublets and it is directly projected to the input fibre end. A flipping mirror is introduced into the beam for flat fielding and spectral calibration of the spectrograph. In the parallel beam, an atmospheric dispersion corrector (ADC) is placed together with a cube beam splitter. The splitting surface of the beam splitter is coated to reflect 3–4 % of the telescope beam to the acquisition and guiding camera. The back side of the cube is coated in order to send the image of the fibre and star on the guiding camera. This layout doesn't need the traditional pinhole-mirror in front of the fibre. In our case, the pinhole should have been 40 μm which is difficult to manufacture and expensive. However, a small silica plate coated with an antireflection coating must be glued to the fibre end to reduce the Fresnel losses.

Table 1. Marvel fibre link specifications.

Fibre sky aperture	2.29 arcsec
Fibre focal ratio	Injection: $f/4.5$ Output: $f/4$
Spectral range	390 – 920 nm
Photometric scrambling Far field (pupil illumination ratio) Near field (scrambling gain)	Combination of a circular and an octagonal fibre < 20 % peak to peak variations RV 1m/s, SG > 300
Circular fibre Octagonal fibre	40 μm . UV grade; 5 – 10 m 40 μm side-to-side. UV grade; 5 m
Circular-octagonal coupling Coupling matching refraction index Coupling efficiency ($f/4.5 - f/4$)	Optical gel > 90 % (focal ratio degradation included)
Fibre link efficiency	> 55% at 390 nm > 65% at 420 nm > 75% 500 – 920 nm range

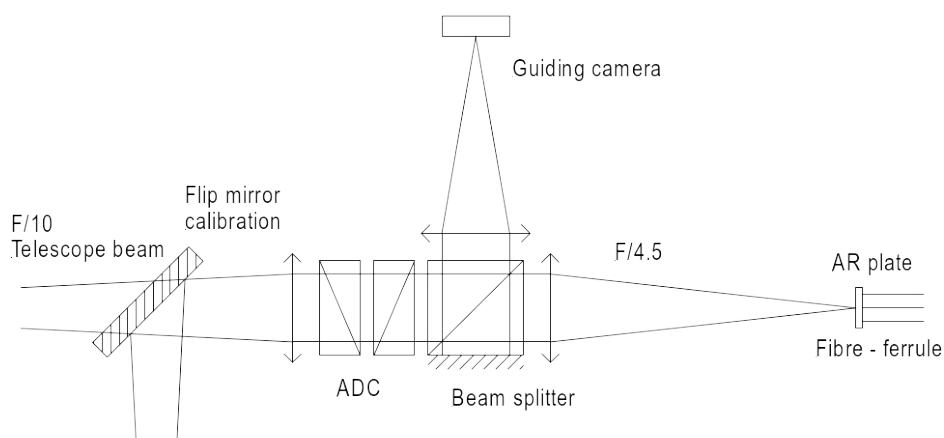


Figure 2. Injection of the telescope beam into the fibre input end.

As for the injection to the spectrograph, a proposed rod lens glued to the fibre end and a triplet will produce a real focus at the slit plane of the spectrograph's input collimator.

3. FOCAL RATIO DEGRADATION OF CIRCULAR, OCTAGONAL FIBRES AND COMBINATIONS

A systematic number of measurements on four fibres were performed at the Baader Optical Lab. The fibres were three circular of 3 m each with a core diameter of 40 μm , a cladding of 56 μm and a polyimide buffer of 68 μm . All of them are from CeramOptec series UV/WF and with a NA of 0.22. The fourth fibre was octagonal from Polymicro series EFBP with NA 0.22 and core/clad/polyimide buffer of 40/125/140 μm respectively. The length was 5 m.

Figure 3 shows the optical layout and photo of the setup used for the measurement of the focal ratio degradation (FRD). A bright, broadband and high stable LED centered at 550nm was used as a light source. The LED was directly coupled to a 100 μm fibre and the output fibre end was placed at the focal plane of a doublet with 200 mm focal distance. A wheel with iris apertures was used to define the $f/\#$ of the injection beam into the test fibre. A beam-splitter sends around 50% of the flux to a reference integration sphere with a photodiode integrated and the transmitted beam is focused into the test fibre with a 50 mm focal distance doublet. An auxiliary doublet of 200 mm focal distance was used together with an eyepiece to check the position of the image of the 100 μm fibre end with respect to the core of the test fibre.

The diameter (theoretically 25 μm) of the projected spot on the input fibre end was measured. Its FWHM was 30 μm . It almost covers the surface of the 40 μm fibre core but still smaller enough to be sure that all the flux enters into the fibre. By measuring the total flux of the spot without fibre, this experimental setup allows to measure the absolute fibre efficiency. The reflected beam by the beam-splitter is focused to a second integrating sphere and it is used as a reference beam to monitor the flux variations of the light source.

The output end of the test fibre is projected to a couple of doublets and iris wheel to precisely define the output $f/\#$. An integrating sphere containing a photodiode measures the flux from the fibre. The relative FRD is obtained by normalizing the flux at a given $f/\#$ to the flux obtained by the maximal diameter of the iris available. The highest aperture is $f/2$, large enough to the $f/2.22$ generated by the standard numerical aperture (NA) of 0.22.

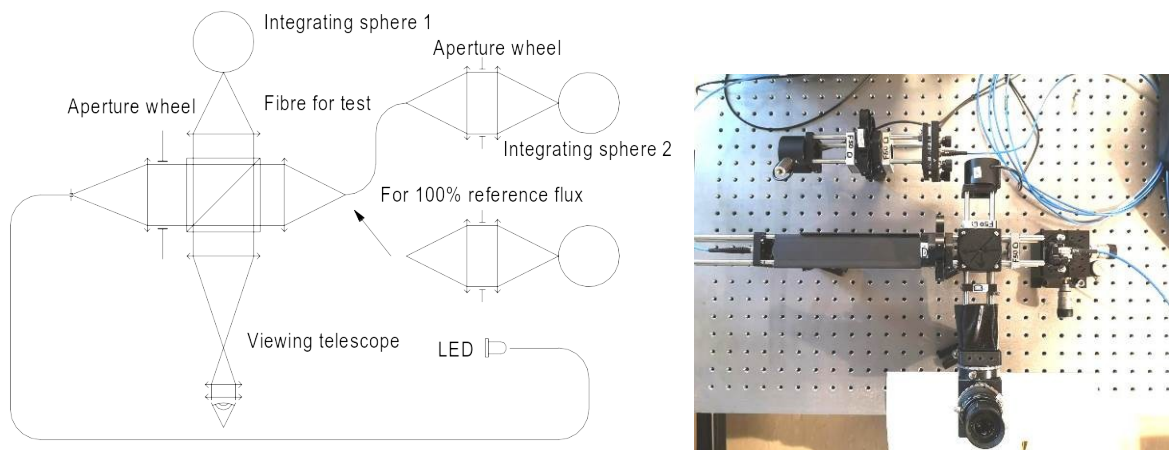


Figure 3. Optical layout for the measurement of the focal ratio degradation.

The numerical aperture of the fibre defines the maximal angle of an input ray which can be transmitted along the fibre. Since this is valid for any point on the surface of the input fibre end, all the rays are telecentric with respect to the fibre, in other words the pupil is at infinity with respect to the fibre ends. This is the reason why the telescope-to-fibre coupling optics has to be telecentric. Out of this condition, there is vignetting of flux by the fibre, but by how much?

In addition, in our optical setup, it is difficult to put exactly the iris on the focal plane of the 50 mm injection lens, in consequence the pupil with respect to the fibre is not at infinity. We calculated the amount of vignetting in the fibre when the pupil is at a finite distance from the fibre input end.

Figure 4 shows a pupil illuminating a pinhole acting as a fibre core and a screen to project the rays which pass the fibre core.

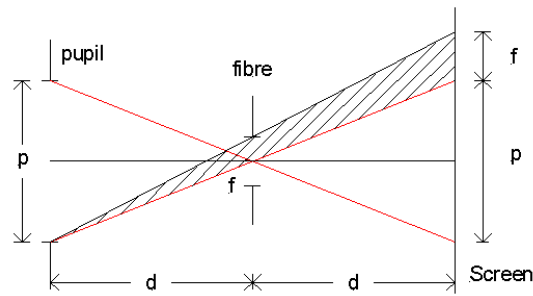


Figure 4. A pupil at finite distance from the fibre input end.

The red lines defined the telecentric rays entering into the fibre at the centre of the core. In order to simplify the calculation, the screen is placed symmetrically with respect to the fibre pinhole. All the rays included in the hatch zone are not telecentric and therefore out of the input $f/\#$ aperture, in other words, they are vignetted.

Figure 5 shows the Zemax calculation of the fibre coupling efficiency with respect to n , which represents the pupil to fibre diameter ratio. It was simulated for a beam aperture of $f/4$ but further calculations show that it is independent of the $f/\#$.

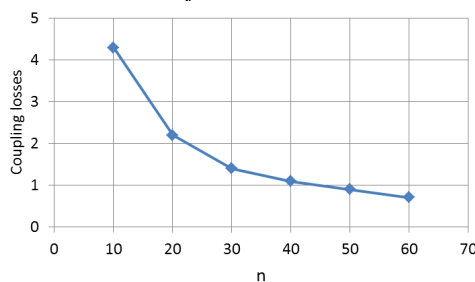


Figure 5. Fibre efficiency losses when the pupil is placed at finite distance from the fibre input end. n is the pupil to fibre diameter ratio.

When the pupil is 50 times the fibre diameter the coupling loss efficiency is only 0.9%. In the case of the MARVEL fibres, their core is $40\ \mu\text{m}$ and therefore the pupil should be at least 2 mm. The distance pupil – fibre will be $f/4.5 \times 2\ \text{mm} = 9\ \text{mm}$. In our experimental setup, the smallest pupil diameter which defines $f/6$ beam is around 20 mm, well beyond the 2 mm required for a vignetting below 1%. This criterion is very useful when designing the optics to couple the telescope beam into the fibre. For practical design purposes a pupil more than 60 times the fibre core is a safe margin to ensure vignetting below 1%.

An important adjustment for optimal measurements is the orientation of the input fibre end with respect to the injection beam. Usually there are two possibilities: first, the incoming beam is not arriving parallel to the fibre axis and second, the surface of the fibre end was polished with a certain angle with respect to the fibre axis. These possibilities are illustrated in Figure 6.

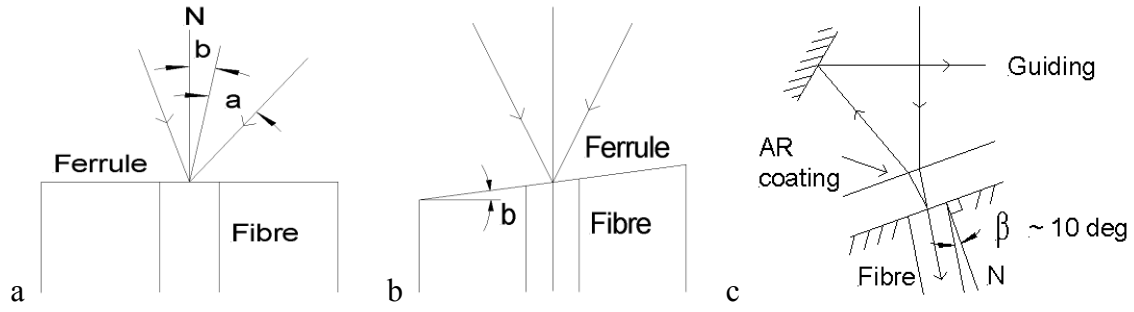


Figure 6. Injection of the telescope beam into the fibre input end

In the first case, the incoming beam which is defined by the demi-angle a , arrives at the fibre end with an angle error b . The fibre will “see” a beam with an equivalent demi-angle of $a + b$. If F is the f-number of the incoming beam, the degraded new beam aperture F' at the output of the fibre will be given by the equation (1).

$$F' \approx \frac{F}{1+2bF} \quad (1)$$

In the second case, if n is the refraction index of the silica at a given wavelength, the degraded F' at the output of the fibre will be (equation 2):

$$F' \approx \frac{F}{1+2b(n-1)F} \quad (2)$$

In our case, the incoming beam is opened to $f/4.5$, if the incoming beam is tilted by only 1 degree, the aperture degrades very fast: $F' = 3.9$. In the second case, if the fibre end is polished with 1 degree with respect to the mechanical axis of the ferrule, the degradation is less critical: $F' = 4.2$.

For correction of these misalignments, a laser beam is injected from the output fibre side and the projection of the beam is aligned with respect to the incoming beam using a semi transparent screen. When the telescope beam is directly launched on the fibre input end, there are two factors contributing to the coupling losses to the fibre: the Fresnel reflection (3.6% for silica) and the polishing quality. The fibre end can be coated with an anti-reflection (AR) layer, however, this coating is fragile and costly, and in addition the polishing errors remain. Another solution is to glue a thin silica plate in front of the fibre. The plate is AR coated on the input surface and aluminized on the other side but not on the fibre core. This aluminization around the fibre core creates a pinhole which allows tracking the position of the star in front of the fibre core. If the plate-fibre is inclined to send the telescope beam to an acquisition/guiding camera, the fibre must be slightly inclined with respect to the plate normal to avoid increase of FRD as shown in c of Figure 6. Indeed, the incoming beam must be parallel to the fibre axis. In the case shown in the figure, the incident beam is tilted by 30 degrees and therefore the fibre should be tilted by 8 degrees with respect to the normal of the plate.

It is important to point out that the relative FRD is the well-known parameter to compare the preservation of the beam aperture of different fibres or combination of fibres. The absolute FRD which takes into account the real throughput of the fibre is used to detect “anomalies” which cannot be deduced from relative measurements. The total fibre efficiency can be low but the relative one can be very high! This is the obvious case of fibres with low NA like 0.1 ($f/5$) when illuminated by beams with $f/\#$ lower than $f/5$. Figure 7 shows the Absolute FRD of a 25 μm fibre, 5m long and NA

0.1. The relative FRD for an $f/4$ input beam is almost 100% while the total transmission is only 37%.

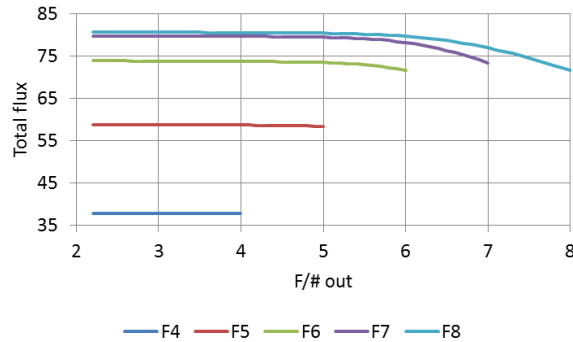


Figure 7. Total focal ratio degradation of a 25 μm fibre, 5m, NA 0.1

Another typical case is when the clad of the fibre is very thin (less than 5 μm). The FRD is highly dependent on the wavelength.

Coming back to the MARVEL circular fibre, Figure 8 shows its total and relative FRD.

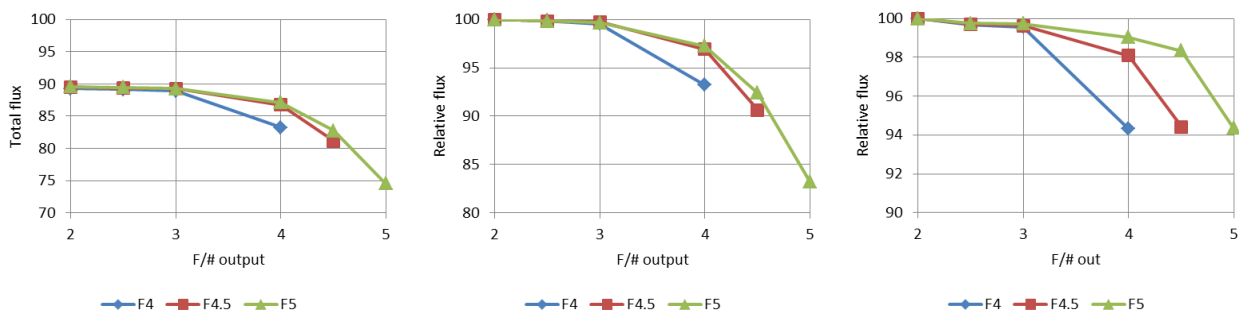


Figure 8. Left: total FRD of a circular 40 μm , 3m fibre. Middle: relative flux. Right: relative FRD of the octagonal 40 μm , 5m fibre

The total transmission of a short fibre should approach 93% where just the Fresnel losses produced by silica are taken into account. However, we measured only 89.6% at the fibre output end with a detector opened to $f/2$ as shown in the left plot of Figure 8. The additional losses are due to at least three reasons: low polishing quality of the fibre ends, leakage of flux beyond the NA at the fibre output end and dispersion of light all along of the fibre by manufacturing failures (impurities, inhomogeneity and core to clad interface imperfections).

In order to test the polishing quality, we repeated the total efficiency at $f/2$ at the output of the fibre by placing a small drop of distilled water on the fibre ends. We obtained an efficiency of 91%.

It is remarkable the low FRD by the octagonal fibre with respect to the circular counterpart: 94.2% for $f/4$ to $f/4$ and 91% for the circular fibre under the same conditions.

Table 2 shows a summary of FRD results in the cases: absolute and relative efficiency. As previously pointed out, the absolute efficiency takes into account all contributions: fibre

transmission, Fresnel losses, dispersion beyond the NA, FRD and end surface polishing quality while the relative efficiency considers only the FRD.

Table 2. FRD of circular and octagonal fibres.

	Absolute (%)		Relative (%)	
	$f/4.5-f/4.5$	$f/4.5-f/4$	$f/4.5-f/4.5$	$f/4.5-f/4$
Circular	81.3	86.7	90.6	96.9
Octagonal	83.2	86.4	94.4	98.1

The octagonal fibre 5m sample from Polymicro gave an excellent relative FRD: 98.1% ($f/4.5$ to $f/4$). However, the gain in flux with respect to the configuration of $f/4.5$ to $f/4.5$ is only 4% (from 94.4 to 98.1).

In order to compare the efficiency between fibres with similar lengths it is not practical to use the absolute FRD but the relative one since the polishing quality highly varies from fibre to fibre. The other parameters like manufacturing limitations are quite similar. Checking the table, we confirm that the octagonal shows a lower FRD.

It is important to point out that the flux distribution of the far field of our fibres shows a strong dependency with the injection spot diameter. The pictures of the far field in the section below show a high concentration of flux in the centre of the image when illuminated with a 16 μm spot. This effect reduces the FRD and extrapolating these results at the telescope, the FRD will be highly dependent on the seeing quality.

The next step was to test the combination of the circular and octagonal fibres. We started with the measurement of their coupling efficiency. A high precise coupler (Figure 9) was used to approach the fibre ends. It included fine adjustment on the lateral, tip-tilt and focusing movements of one fibre with respect to the other.

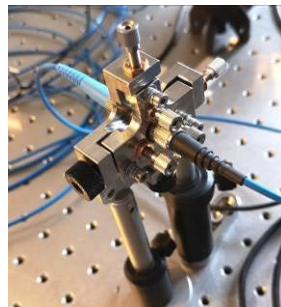


Figure 9. Circular - octagonal fibre coupler

Table 3 shows the results obtained under different conditions. First, an $f/3$ beam carrying a 50 μm spot (bigger than the fibre core) was used for uniform illumination of the fibre input end. Then we exchanged the $f/3$ beam with our working $f/4.5$ beam. Later we reduce the incoming spot to 30 μm (fibres are 40 μm) to check the effect of the flux confinement along the fibres. In this case, we placed the spot at the centre of the fibre end and then at the edge. The light source was a broadband LED at 550 nm.

Table 3. Coupling efficiency between the circular and octagonal fibres.

	Circular to octagonal (%)	Octagonal to circular (%)
Spot bigger than fibre and $f/3$ beam	93.9	
Spot bigger than fibre and $f/4.5$ beam	95.7	90.1
30 μm spot, at centre and $f/4.5$	99.0	95.8
30 μm spot fibre, at edge and $f/4.5$	98.7	96.7

In the case where the fibre core is totally illuminated, the coupling efficiency is higher for an $f/4.5$ beam than a $f/3$ beam. Indeed, at high incidence angles and due to the FRD some rays go beyond the numerical aperture. When exchanging the big spot by a smaller one that is fully inside the core of the fibre and placed at the centre, the coupling efficiency clearly increases. Indeed, the flux transmission along the fibre when illuminated by a small spot tends to confine the flux along the centre of the fibre and the coupling efficiency is less sensitive to lateral misalignments. Finally, when the spot is placed at the edge of the fibre core, the resulting efficiency should decrease for any configuration. It was the case for the circular to octagonal combination but not for the octagonal to circular one.

The resulting FRD of the assembly of two fibres is defined basically by two factors: the highest FRD of the individual fibres and the parallelism error of the axis of the individual fibres at the coupler. It is analogous to the entropy of a system, the FRD in a fibre or any configuration with additional optics will always increase. It is also important to point out that the coupling efficiency is quite sensitive to the parallelism error of the optical axes of the two fibres in contact at the coupler. It is the same case discussed following Figure 6 and equation [1]: when the beam of the first fibre illuminates the second fibre with an inclination error with respect to the fibre axis, the cone angle of the incidence beam will increase by this error angle and therefore there will be an increase of the global FRD. In order to minimize the FRD of the combination of two fibres, we have to choose the fibre ends to be in contact showing the minimum parallelism error between the emerging beam and the axis of the ferrules.

Figure 10 shows the relative FRD of the two octagonal and circular configurations.

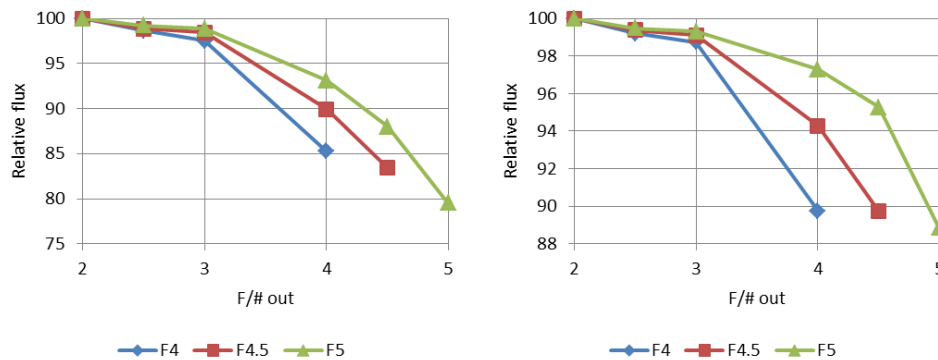


Figure 10. Left: Relative FRD of the octagonal to circular fibre configuration. Right: Circular to octagonal configuration

Note that the behavior is similar to the exit fibre. In the circular to octagonal combination, the FRD is almost independent of the FRD of the input beam. Table 4 shows the summary of the test results.

Table 4. FRD of combination of circular and octagonal fibres.

	Absolute (%)		Relative (%)	
	$f/in - f/out$		$f/in - f/out$	
	$f/4.5 - f/4.5$	$f/4.5 - f/4$	$f/4.5 - f/4.5$	$f/4.5 - f/4$
Octagonal to circular	72.1	77.8	83.4	89.9
Circular to octagonal	76.7	80.6	89.7	94.3

The combination circular to octagonal fibres show the best relative FRD: 94.3%.($f/4.5$ to $f/4$) with a gain of flux of 5.1% with respect to the $f/4.5$ to $f/4.5$ apertures.

We have decided to inject an $f/4$ beam into the fibre and to collect an $f/4$ beam at the output end in order to increase the fibre efficiency at the expense of reducing slightly the resolving power. It is a resolution vs. efficiency trade-off that depends on the seeing conditions at the observatory and the features of the particular fibre link. Table 5 outlines this trade-off for the MARVEL fibres.

Table 5. Resolution vs fibre efficiency trade-off.

Seeing (arcsec)	FRD (%)	Resolution ($\lambda/\Delta\lambda$)	Pinhole efficiency (%)	Total flux (%)
	$f/4.5-f/4.5$			
1	89.7	101 000	0.974	87.4
2	89.7	101 000	0.6	53.8
	$f/4.5-f/4$			
1	94.3	90 000	0.974	91.8
2	94.3	90 000	0.6	56.6
	$f/4-f/4$			
1	89.7	90 000	0.99	88.8
2	89.7	90 000	0.68	61

The sky aperture of the MARVEL fibres is 2.3 arcsecs, therefore there is a significant difference of the flux gathered by the fibre if the seeing is 1 or 2 arcsec. This range of seeing is common at El Roque de los Muchachos Observatory. In the table, the *Pinhole efficiency* is calculated by the integral of a bi-dimensional Gaussian function (seeing) over a circle (fibre) [9] and the *Total flux* is the product of the FRD by the pinhole efficiency.

In good seeing conditions, the $f/4.5-f/4$ configuration provides the highest flux (91.8%) efficiency, but the resolution is 90 000. With bad seeing, the flux in the $f/4-f/4$ combination is the best option (61%) but again the resolution is low (90 000). If the resolution is privileged to the flux, the $f/4.5-f/4.5$ scheme should be chosen. In this case, the reduction of flux with respect to $f/4.5-f/4$ is 5% for 1 or 2 arcsec seeing. However, if a 2 arcsec seeing is persisting at the observatory, the $f/4-f/4$ should be adopted. The flux gain with respect to the $f/4.5-f/4.5$ is 13% at 2 arcsec but a reduction of resolution of 11%. It is up to the science board to decide the final configuration.

To finalize the FRD study on MARVEL fibres, we present a summary of the variation of the FRD in Table 6 when the spot moves from the centre to the edge. The later position roughly simulates a complete illumination of the fibre core. Indeed, at this position and by rotational azimuth transmission all the rays scramble to simulate, in principle, a total illumination of the fibre.

Table 6. Change of FRD with input illuminating spot diameter.

	Increase of FRD (%)
Circular	0.5
Octagonal	1.4
Octagonal to circular	0.4
Circular to octagonal	-0.3

In most cases there is an increase of the FRD as expected but not in the case of the circular to octagonal arrangement, where there is a slight decrease of the FRD.

4. NEAR AND FAR FIELD PHOTOMETRIC SCRAMBLING

Since the fibres have a small diameter, the number of transmission modes is relatively “small”: $M = (\pi d NA / \lambda)^2 \sim 1500$ at $\lambda = 0.5 \mu\text{m}$, $NA 0.22$ and $d = 40 \mu\text{m}$. Therefore the scrambling properties start to be sensitive to the modal noise. In order to measure the scrambling gain (SG) taking into account the modal noise, a light source with a narrow band spectral band was used for the tests.

In order to measure the near field scrambling gain of a fibre, we use the traditional ratio of the displacement of the spot in front of the input fibre to the displacement of the barycenter of the image of the output fibre end on the detector, equation (3).

$$SG = \frac{d/f}{D/F} \quad (3)$$

Where: d is the displacement of the spot inside the fibre core, in our experimental setup it is $12 \mu\text{m}$; f = fibre diameter = $40 \mu\text{m}$; D = shift of the centre of mass of the image of the core fibre in CCD pixels and F = diameter of the image of the core fibre in pixels. This diameter was defined by the FWHM of the image of the core fibre on the detector. It was constant and covered 70 pixels. The utility and scope of this equation has been discussed by other authors, like A. P. Sutherland [4].

As for the far field, it is difficult to find an appropriate expression providing the displacement of the centre of mass of the point spread function with variations of illumination of the spectrograph pupil. Zemax may help to simulate the influence of flux variations on the pupil of the spectrograph on the spot diagram by defining a proper mask vignetting the rays according to the flux variations. Unfortunately I couldn't find a proper way to simulate this mask. As an alternative we took the simple ratio of fluxes at the level of the pupil when the star is in the middle (field 0,0) and when it is at the edge of the fibre core (field 0,1 for instance).

Figure 11 shows the experimental setup for the measurements. It is basically the same as for the FRD but here the light source is provided by a high resolution monochromator illuminated by a power and stable LED centered at 554 nm (Thorlabs MINTL5) with an effective spectral range between 420 and 700 nm.

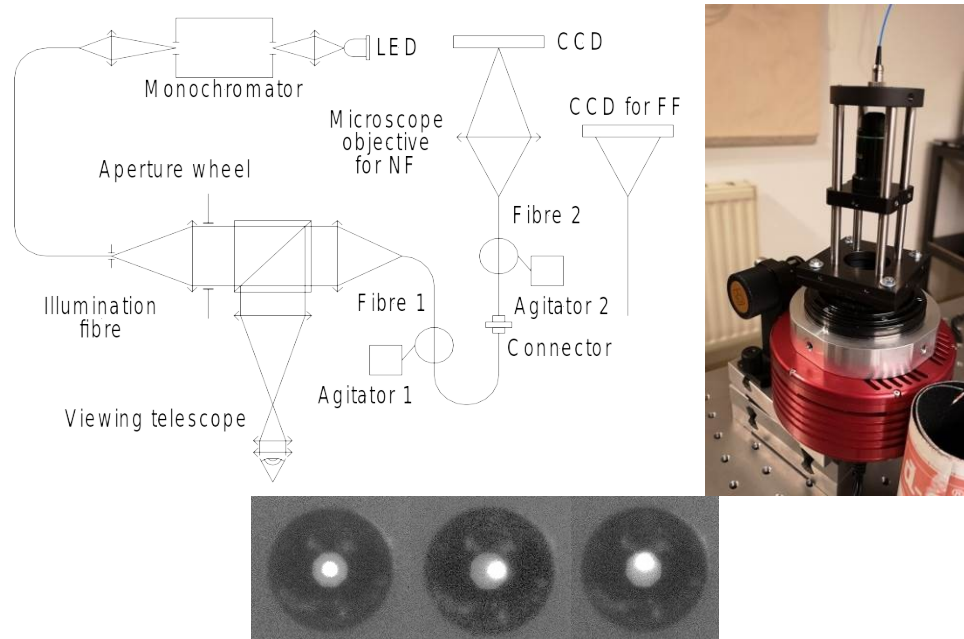


Figure 11. Above: optical layout for the measurement of the near and far field photometric scrambling and picture. Below: pictures of the 40 μm circular fibre input end with 16 μm spot in 3 field positions: 00, 10 and 01

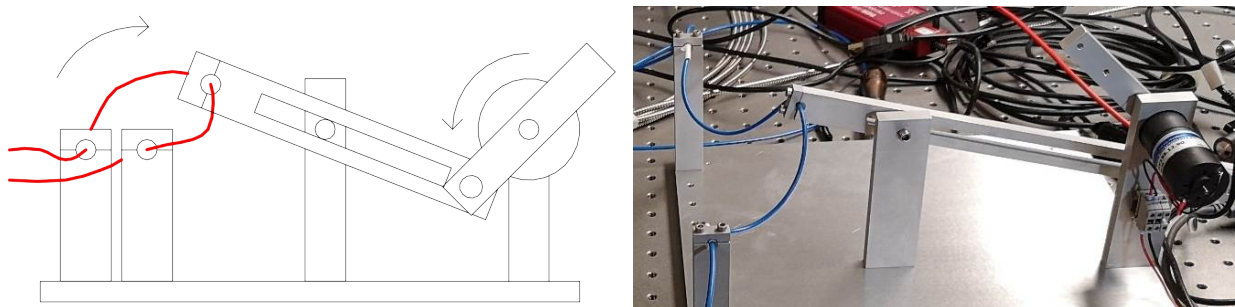


Figure 12. Fibre agitator

The bandwidth of the beam illuminating the fibres was 0.3 nm at 550 nm. The reasons to use a high monochromatic light source were two: first, we try to work as close as possible at the working regime of MARVEL spectrograph and second, to study the behavior of fibres with a core diameter close to the single mode domain.

The sky aperture of the MARVEL fibres is rather large 2.3 arcsec. If the seeing is small, say 1 arcsec, most of the flux is concentrated in the centre of the fibre core. In order to study the scrambling behavior in similar conditions; we used a 16 μm spot projected on the fibre input end.

For the near and far field tests, we placed the input spot at 5 positions: at the centre of the fibre (defined as field 00), at the edge in the X axis but always inside of the fibre core (field 01, as represented by the pictures at the bottom of Figure 11), at the edge of Y axis (01) and the complementary fields, -10 and 0-1.

In order to increase the near and far field scrambling gain, we used mechanical agitators attached to a portion of the fibre as shown in Figure 12. A lever attached to an electrical motor moved the fibre in a near circular movement. The frequency of the agitation was 1 Hz maximum.

Near Field photometric scrambling

The measurements of the scrambling gain were performed by projecting the image of the test fibre on a CCD with a 16x microscope objective. In order to increase the mechanical stability of the image of the fibre on the detector, we attached the optical bench containing the objective and fibre to the camera and placed it in a vertical direction (Figure 11). The CCD camera has no shutter. The fibres were attached to the optical table to avoid any movement of the fibre close to the microscope objective. Each batch of exposures was done in a short time to avoid changes of room temperature. The temperature in our lab is quite constant: we measure variations of less than 0.1 degree per hour. For each field position we took 10 samples per field position.

Figure 13 shows images of the circular and octagonal fibre output ends illuminated with a 16 μm spot in polychromatic and monochromatic regimes. First, the spot is at the centre of the fibre core (field 00) and then displaced at the edge (field 10).

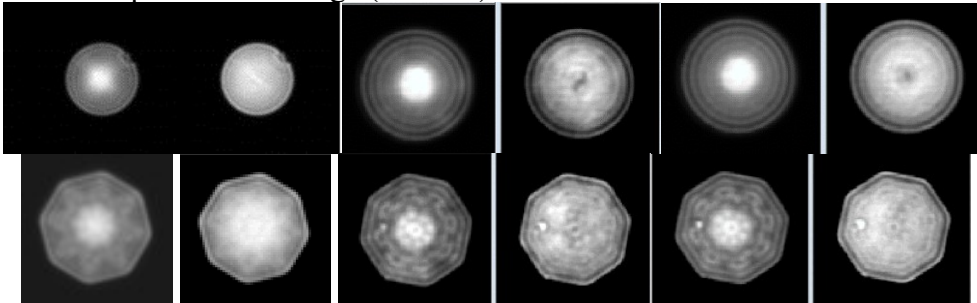


Figure 13. Above: Near field of circular fibre. From left: broadband illumination spot at fields 00 and 10. The next two pictures are the same but the spot is monochromatic. In the last two pictures, the agitator is ON. Below: octagonal fibre illuminated in broadband with the spot on the centre 00 and field 10. In the next two pictures, the illumination is monochromatic and the spot is at the centre and on the field 10. In the last two pictures, the agitator is ON.

When the spot is placed at the centre (field 00) the images of both circular and octagonal fibres show a remarkable concentration of the flux in the centre of the cores. The flux is confined all along the fibre. Given the small core of the fibre, the light propagation along the fibre does not follow exactly a geometrical ray behaviour, it starts to show some cavity modal transmission properties.

This is not the case for bigger fibres. Figure 14 shows the near fields of 3 octagonal fibres: 67 and 70 μm diameters where the spot is at field 00. The illumination distribution on the fibre surface is quite flat. The next two pictures are subsequent exposures of the MARVEL 40 μm fibre taken immediately one after the other. We can see the modal noise between the two pictures even if the fibre is at rest on the optical table. The last picture is the subtraction of the previous images to enhance the modal noise. The plot is a line profile of the two images. It is important to point out that the flux changes rapidly and therefore the scrambling gain. In order to average the modal noise, we took 10 exposures of 3 seconds each for every field.

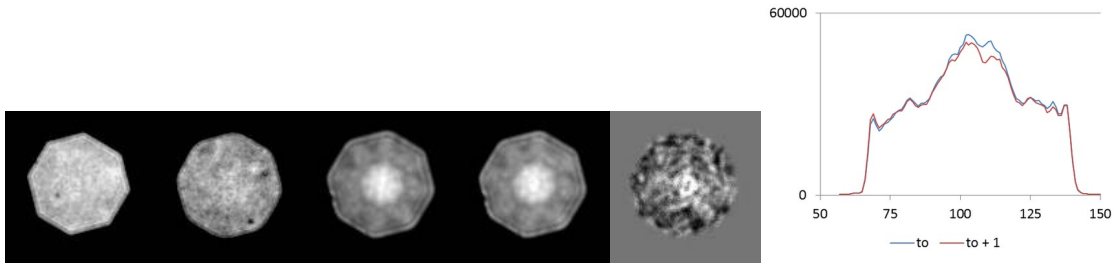


Figure 14. Near fields of 3 octagonal fibres illuminated with a $16 \mu\text{m}$ spot in the centre and with monochromatic light. From left: 67, 70 and $40 \mu\text{m}$. The fourth image is a second exposure of the 40 taken without delay. The last picture is the subtraction of the last two images. The plot is the profile of a horizontal line passing by the centre of the last two images

Table 7 lists a summary of the scrambling gain of the circular and octagonal fibres.

Table 7. Scrambling gain of circular and octagonal fibres.

Field	Circular fibre			Octagonal fibre	
	Broadband	Narrow band		Narrow band	
	Agitator OFF	Agitator OFF	Agitator ON	Agitator OFF	Agitator ON
1,0	430	46	103	38	113
-1,0	604	74	277	136	73
0,1	406	47	94	84	157
0,-1	663	232	277	78	81
Average	526	100	188	84	106

The SG is quite high (526) when the circular fibre is illuminated with a large band wavelength range (420 – 700 nm). However when the fibres are illuminated with a narrow wavelength band, the SG is much lower. When the agitator is in operation the SG increases notably. But it doesn't reach the values using a broadband illumination.

The next step was to test the scrambling efficiency of the combination of the circular and octagonal fibres. Figure 15 shows the near field of the two combinations, octagonal to circular first and circular to octagonal. In all pictures, the agitator is ON. On the left picture of the first couple, the spot is at the centre and the agitator is attached to circular fibre. In the next picture the spot is at field 10. In the next couple, the agitator is acting on the octagonal fibre for fields 00 and 10. Note that the concentration of flux is always present in the centre of the fibre in spite of the agitator. However, it is better scrambled when the agitator acts on the octagonal fibre. The last two couples of pictures show the circular to octagonal arrangement with the same conditions as the previous combination.

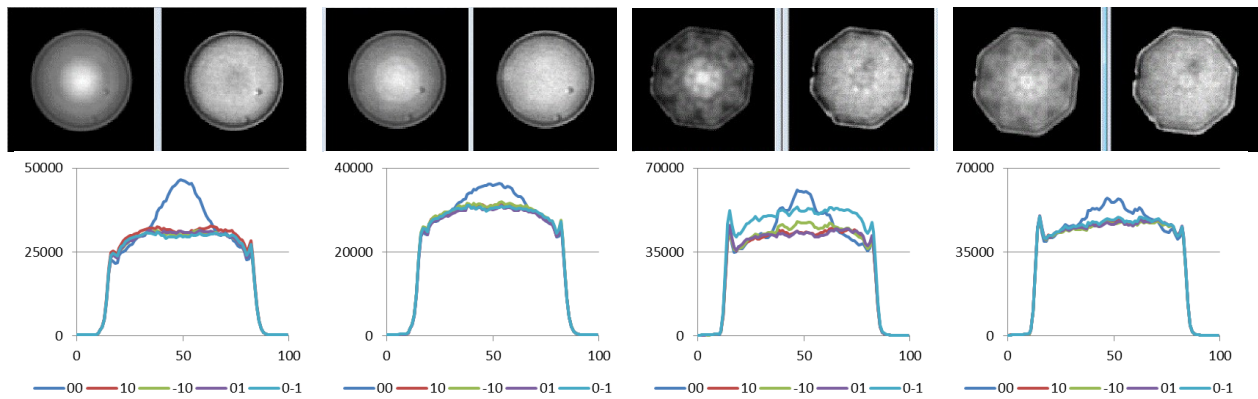


Figure 15. Each couple of two pictures above show fields 00 and 10. First two couples: octagonal to circular. First couple: agitator on the circular fibre, then agitator on the octagonal. Last 2 couples: circular to octagonal. First couple: agitator on circular and then agitator on octagonal. Plots: line profiles for each case as described for the pictures but including all fields

The line profile plots include all fields: the first one corresponds to the octagonal to circular combination when the agitator is on the circular fibre, the second when the agitator is on the octagonal fibre, the third is for the circular to octagonal configuration when the agitator is on the circular and the last one when the agitator is on the octagonal fibre.

Table 8 summarizes the SG for the octagonal-circular pair when the agitators are OFF and then ON.

Table 8. Scrambling Gain octagonal to circular in static/agitation modes and monochromatic illumination

Field	Agitators OFF	Agitators on both fibres
10	177	1020
-10	139	962
01	237	426
0-1	202	702
Average	189	778

As expected, the SG is quite sensitive to the agitators. Table 9 shows a detailed SG for different cases of the circular to octagonal combinations.

Table 9. Scrambling gain of the near field of the circular to octagonal combination.

Field	Agitator OFF	Agitator on circular	Agitator on octagonal	Agitators on both fibres
10	193	886	920	1124
-10	162	307	830	1498
01	125	346	737	3015
0-1	129	398	564	1322
Average	152	484	763	1740

Comparing all results, we concluded that the SG is higher for the circular to octagonal combination with both agitators in operation.

In the next test, we wanted to check the scrambling properties of the octagonal to circular combination when illuminated by different wavelengths: at 475 and 640 nm. Figure 16 shows the results for three fields: -10, 00 and 10. The upper near fields correspond to 475 nm and the row below to 640 nm.

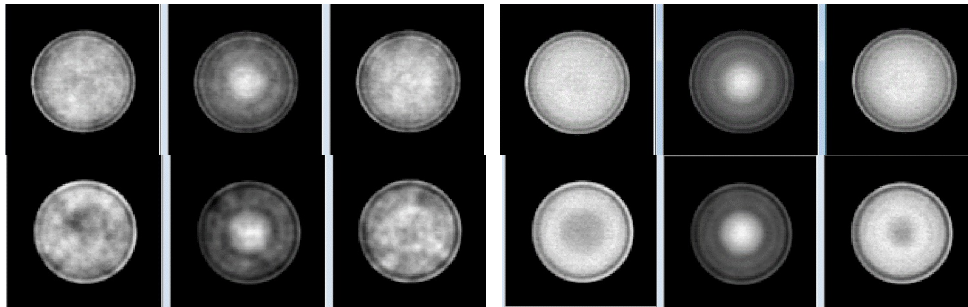


Figure 16. Octagonal to circular showing -10, 00 and 00 fields. Above: 16 μm spot at 475 nm wavelength in narrow band. Left: agitators OFF, right: agitators ON on both fibres. Below: same spot at 640 nm narrow band. Left: agitators OFF, right: agitators ON on both fibres.

As expected the increase of modal behavior is evident at red wavelengths. In the pictures of the 3 left columns, the agitators applied to both fibres are OFF. For the right 3 columns, the agitators were ON. The reduction of modal noise is clear.

In order to study the scrambling gain with respect to the position of the spot on the fibre core, we have scanned the spot along the x-axis. The 32 μm travel between the centre and the edge (the 16 μm spot is touching the edge of the fibre core) was divided in 10 steps, i.e. 3.2 μm each (Figure 17).

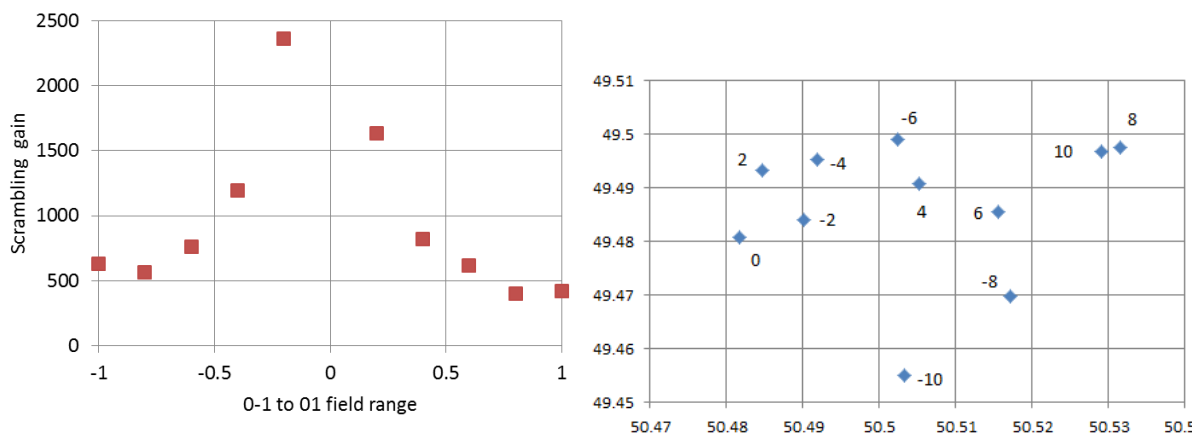


Figure 17. Variation of the SG when the input spot sweeps the x axis (-10 to 10). The agitator was applied to the octagonal fibre (octagonal to circular configuration). Right: Centre of mass for each field. The CM for the field 00 has been added

The SG is not symmetrical with respect to the field 00. Indeed, the near field patterns have different developments along the scanning and we found that is related to the shape of the fibre path on the optical table. The right plot in the figure shows the position of the centre of mass of the image of the fibre and confirms this asymmetry where the points with symmetric positions are at different places. In addition, the shape of the SG curves follows the hyperbolic behavior of the equation of the SG.

Far field photometric scrambling

Figure 18 shows the far field produced by the circular fibre when the spot is at the centre and at field 10. In the first couple of exposures, the illumination is broadband and narrow band for the others. In the second couple, the agitator is OFF and ON in the last couple.

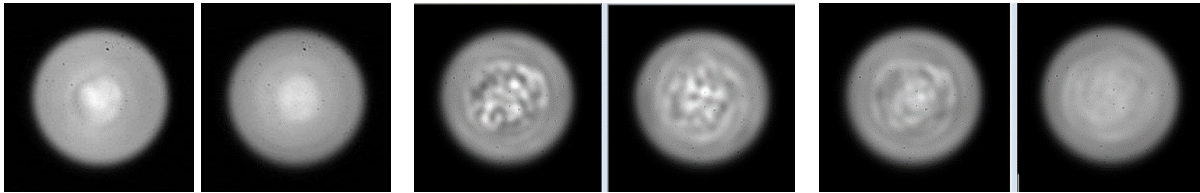


Figure 18. Far field of circular fibre with injection spot of $16\ \mu\text{m}$ at $f/4.5$. From left: fields 00 and 10 in large band. Next two pictures are the same but in narrow band. Last two, narrow band and agitator ON

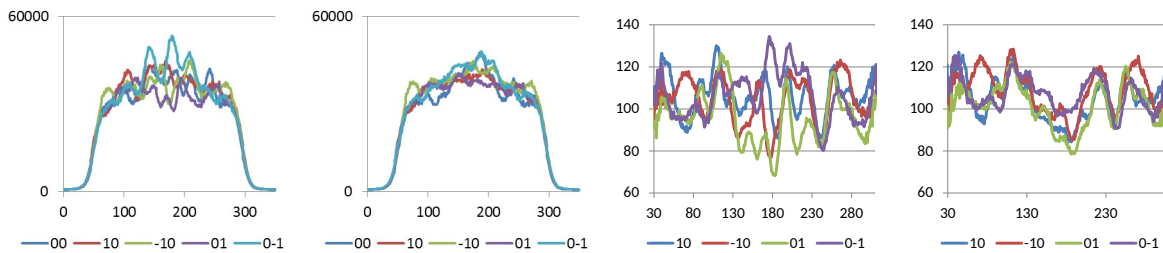


Figure 19. Line profiles of the far fields of previous figure in narrow band illumination. In the first 2 plots, the agitator is OFF and later ON. The right plots show the ratios with respect to field 00 when the agitator is OFF and then ON.

The plots in Figure 19 show the line profiles of the previous figure: in the first, the agitator is OFF, in the second it is ON. The last plots are the ratios of the individual curves for each field with respect to the field 00. The agitator is OFF and then ON. The peak to peak variations of the ratio of far fields is 40 %, well beyond the 20% as required.

Figure 20 shows the far field variations produced by the octagonal fibre with a $16\ \mu\text{m}$ spot for three fields: -10, 00 and 10. In the first row, the illumination is broadband. The agitator is ON in the fourth picture. In the second row, the illumination is narrow band with agitator OFF for the left three exposures and ON for the last three. It is remarkable the concentration of flux in the middle of the far field. The intensity of the central peak in the field 00 reaches the double of the average flux as shown in the plots and it is not attenuated when the agitator is applied. In the last row, the line profiles for the second row pictures are shown. The last two plots are the ratios. Note that the peak to peak variations are quite attenuated when the agitator is in operation, almost by a factor of four!

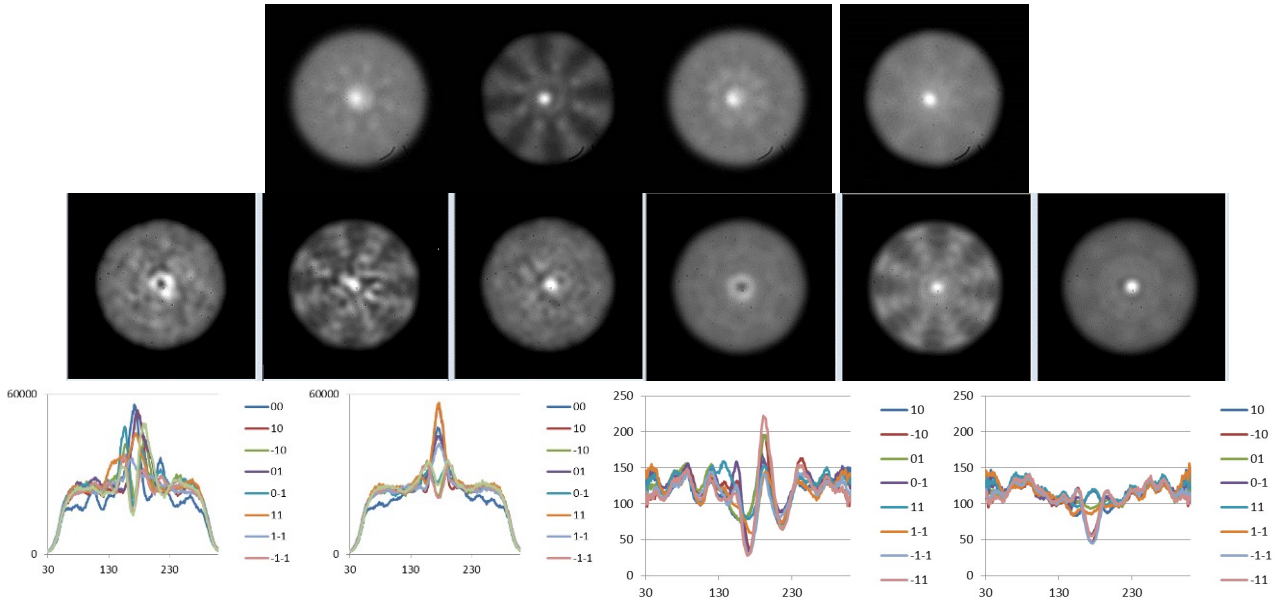


Figure 20. Far field of octagonal fibre with injection spot of $16\ \mu\text{m}$ at $f/4.5$. Top, large band illumination. From left: fields -10, 00 and 10. Last picture: field 0-1 with agitator. Middle: narrow band illumination. Fields -10, 00 and 10 without and with agitator. Bottom: line profiles when agitator is OFF and then ON. Third and fourth plots are field ratios with respect to field 00 without and with agitator respectively.

At the beginning we thought that this was an unusual behavior by these $40\ \mu\text{m}$ octagonal fibres. These enormous variations have not been observed for bigger fibres in *broadband* illumination. It is also commonly admitted that the octagonal fibres should scramble better than circular fibres. We found that the far field ratio variations by the octagonal fibre were much larger than by the circular fibre. Following these results, we tested a $67\ \mu\text{m}$ octagonal fibre under several conditions. The results are plotted in Figure 21.

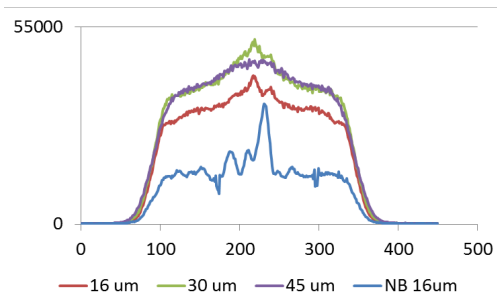


Figure 21. Line profiles produced by a $67\ \mu\text{m}$ octagonal fibre. In the blue curve case, the illumination was narrow band and with an injection spot of $16\ \mu\text{m}$. In the other curves, the illumination was broadband with 3 different spots.

When the fibre is illuminated with a broadband spectral range, the concentration of flux at the centre attenuates with the size of the spot. In a narrow band and with a small spot ($16\ \mu\text{m}$) the concentration of flux highly increases in the centre of the far field.

The far field scrambling generated by the octagonal to circular combination is shown in Figure 22.

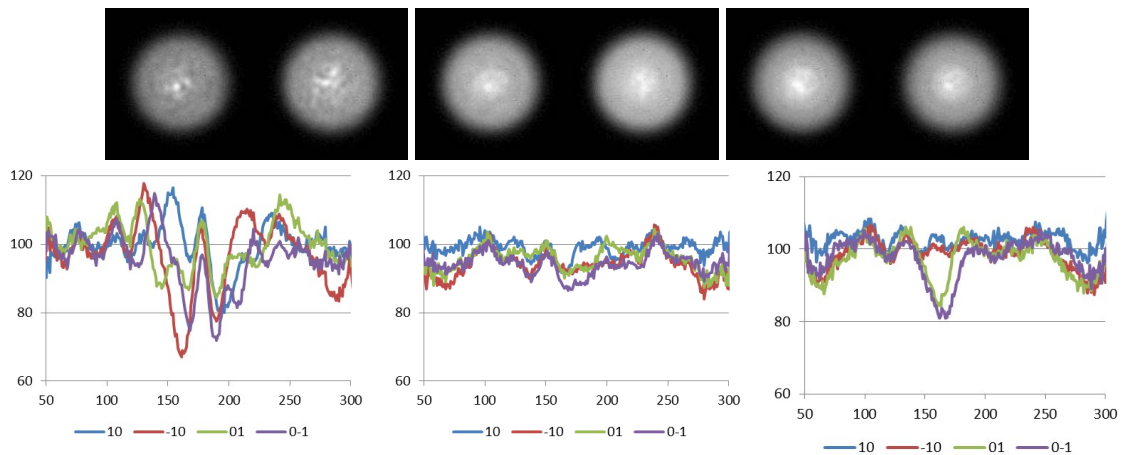


Figure 22. Profiles of FF ratios with respect to 00 field in the octagonal to circular fibres combination. Left: agitators OFF, middle: agitator ON octagonal fibre. Right: agitator ON circular fibre.

The illumination is in a narrow band and only the fields 00 and 10 are shown. The agitator is OFF in the first couple, ON in the second couple and the agitator is attached to the octagonal fibre. In the last couple the agitator acts on the circular fibre. The scrambling is more effective when the agitator shakes the octagonal fibre and the ratio variations are below the 20% peak to peak.

Finally, Figure 23 shows the far field scrambling produced by the circular to octagonal combination. In the same way as in the previous case, the illumination is narrow band and only the fields 00 and 10 are presented.

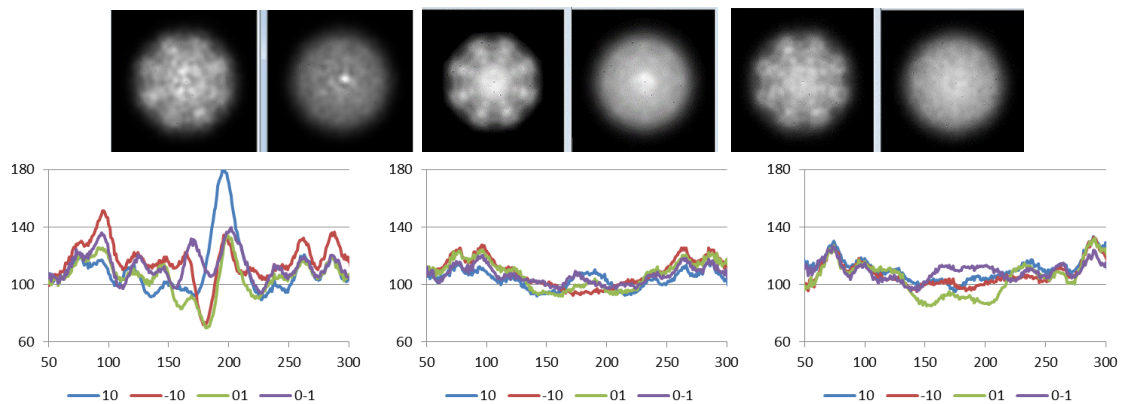


Figure 23. Profiles of FF ratios with respect to 00 field in the circular to octagonal fibres combination. Left: agitators OFF, middle: agitator ON in octagonal fibre. Right: agitator ON on circular fibre

When the agitator shakes the octagonal fibre, the line profiles of the ratios show slightly higher values than the octagonal to circular configuration.

There was the question about how much the agitators would increase the FRD of the fibres. For that we did dedicated tests injecting the monochromatic 16 μm spot for the fields 00 and 10 in the

octagonal to circular configuration. The entrance beam was opened to $f/4.5$ and the detector at the output was set to $f/4$. We have measured the FRD when the agitator was applied to the circular fibre. Comparing the FRDs when the agitator was ON and later when it was OFF we found a degradation of 1.7 % in the worst experimental conditions. In other words, the agitator doesn't substantially increase the FRD of the fibres.

Projection of telescope pupil on fibre input end

Two common methods to couple the telescope beam into a fibre are the projection of the image of the star directly on the fibre input end and the projection of the pupil of the telescope on the fibre end. The latter is practical since a single lens can be used. In particular a gradient index lens of 0.25 pitch where the focal planes lie on the surfaces of the lens as shown in Figure 24. The image of the star is placed on the entrance surface of the lens and the fibre is glued on the rear surface. As the pupil is at infinity, it is projected directly on the fibre. When the star moves out of the centre, the pupil at the output of the fibre shows a typical ring. We wanted to test the scrambling efficiency of this effect using the circular to octagonal configuration and we didn't find any improvement. Figure 24 shows the far fields in narrow band for the 00 and -10 fields. Probably the use of a double scrambler could eliminate the ring by a uniform illumination. Otherwise, the projection of the star on the fibre remains the best option to get the best scrambling.



Figure 24. The telescope pupil is projected on the fibre input end, by means of a gradient index lens of pitch 0.25. The last two images show the far field patterns at the output of the octagonal fibre in narrow band. Fields: 0, 0 (left) and -1, 0.

Optical scramblers

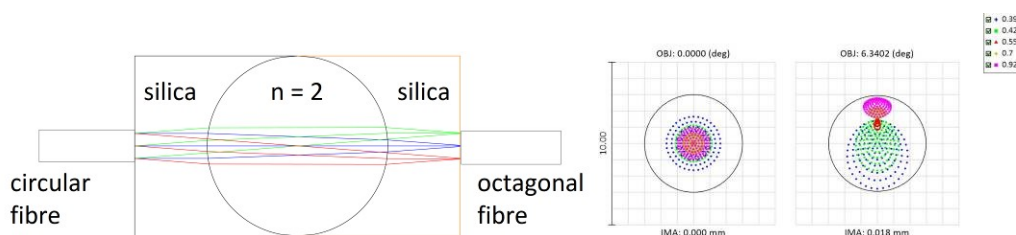


Figure 25. Scrambler with a single ball and spots at the centre and at the edge of the fibre core. The circle is the Airy disc.

In order to increase the scrambling gain, we have explored the use of optical scramblers in our setup. The first idea is to use a single lens like small balls with high refraction index as described in [5 and 6] and illustrated in Figure 25. When the fibre ends are placed at the focal planes of the lens the near end is translated in the far field of the second lens and vice versa. Following our design, $f/4.5$ and 40

μm fibre core, the required focal length of the lens must be $180 \mu\text{m}$! If a ball with refractive index of 2 is used, its diameter should be a bit less than $300 \mu\text{m}$.

In the case of a ball with refraction index of 2, the focal planes lie on the surface of the ball. However, the fibres should be glued in order to reduce the Fresnel losses. In consequence, the focal planes are moved away from the sphere as shown in Figure 25. Thin silica plates glued to the ball and fibres can be used to match the design. In spite of the image quality looks excellent, the lateral chromatism goes away from the octagonal fibre core and the vignetting is increased. The Zemax calculation of the vignetting gives a coupling efficiency of 91%. If the fibres are directly glued to the same sphere, the vignetting increases and the coupling efficiency falls to 82%.

The second possibility is to use the well-known double scrambler composed by a couple of doublets to exchange both the far and near fields. This arrangement is very effective for both throughput and scrambling efficiency. However, in our particular case where the size of the fibre is very small ($40 \mu\text{m}$) and the low beam aperture ($f/4.5$), the design requires lenses with an excellent image quality. For lenses with 5mm focal length, the separation between the doublets is around 250mm. Therefore a precise alignment and mechanical stability are highly required. These requirements would result in an expensive opto-mechanical device. As an alternative we are exploring an inexpensive and compact double scrambler made with gradient index rod lenses (GRIN). In addition it would replace the mechanical coupler. Figure 26 shows the Zemax simulation with commercial GRIN rods of 0.25 pitch, 0.35 mm diameter and 2.14 mm length.

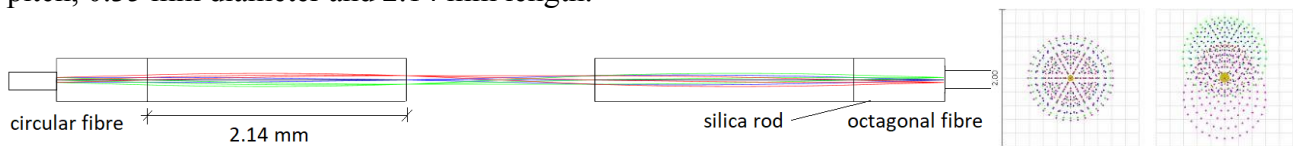


Figure 26. Scrambler with two commercial gradient index rods and silica plates to glue the fibre ends. The scale of the spot plot is just $2 \mu\text{m}$.

A thin silica plate is required to glue the fibre ends on the focal plane of the lenses. The total track of the scrambler is only 9.2 mm. As for the image quality, the plot shows the spot diagram at the centre of the field and to the edge of the fibre core. The scale of the plot is only $2 \mu\text{m}$! We will evaluate a prototype in the coming weeks.

Scrambling of the fibre modal noise

In order to reduce the modal noise in MARVEL fibre link, we used our agitator as a fibre scrambler. We injected our $16 \mu\text{m}$ spot illuminated by a 633 diode laser into the centre of the circular to octagonal fibre link. Figure 27 shows the far fields when the agitator is OFF and then when is ON. The pupil illumination variations are softened but with a high concentration in the centre. In order to have an efficient modal noise reduction, the fibre must be scrambled at high frequency. The period of the agitator is about 1 Hz, so our present scrambler is convenient for observations lasting more than a few seconds.

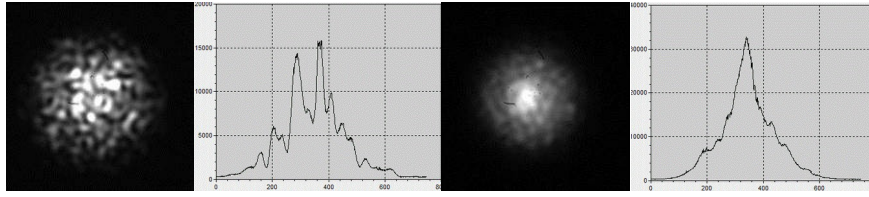


Figure 27. After coupling from circular fibre into octagonal fibre, the left image and profile pair is seen with the agitator off, and the right pair with the agitator on.

Fibre link performances

Table 10 lists the expected fibre link efficiency at 5 wavelengths. We considered the input and output optics together with AR coatings, the internal fibre transmission, the coupler efficiency and the FRD ($f/4.5$ input to $f/4$ output).

Table 10. Scrambling gain of circular and octagonal fibres

Wavelength (nm)	Transmission (%)				
	390	400	500	700	920
Fibre internal transmission (10m, FBP)	91	92	96.3	98.7	99.1
Input and output optics	78	83	92	93	93
Circular-octagonal coupler efficiency (including FRD)	92	92	92	92	92
Total	65	70	81	84	85

The throughput at 390 nm is quite low due mainly to the fibre attenuation and the glasses of the lenses associated with the fibre ends. We are working to find glasses with better transmission in the near UV.

5. CONCLUSION

We have tested the focal ratio degradation and scrambling gain of the proposed 40 μm circular and octagonal fibres for the MARVEL link. We found that the octagonal fibre shows less FRD than the circular fibre. Similar results were found with other octagonal fibres. When combined with a circular fibre, the FRD depends strongly on the parallelism error of the fibre axes at the coupler. In addition, the circular to octagonal configuration showed the minimum FRD.

In order to increase the photometric scrambling, we tested the combinations of octagonal to circular and circular to octagonal fibres. We did the tests by illuminating the fibres with a spot smaller than the fibre core and with a short spectral band illumination to approach the real conditions of observation with good seeing figures and with a high resolution spectrograph. In addition, we used mechanical agitators to reduce the modal noise. We found that the near field scrambling gain of the combination of fibres (circular and octagonal) is quite improved with respect to simple fibres. In

particular, the near field SG of the circular to octagonal combination is higher than the counterpart combination. In any case the measured SG is higher than the required specifications.

As for the far field photometric scrambling and in narrow band illumination, a strong concentration of flux at the centre was present for our 40 μm octagonal fibre. This concentration of flux was lower for the circular fibre.

When the octagonal and circular fibres were combined, the far field scrambling gain for the octagonal to circular configuration was a bit higher than the other combination. Since there is not a clear increase of the photometric scrambling, we are going to test a double scrambler made with GRIN lenses. The short focal length of these lenses allows having a compact and inexpensive scrambler.

REFERENCES

1. G. Raskin. et al. MARVEL, a four-telescope array for high-precision radial-velocity monitoring. These proceedings
2. A. Quirrenbach et al., ‘CARMENES: high-resolution spectra and precise radial velocities in the red and infrared’, in Ground-based and Airborne Instrumentation for Astronomy VII, Austin, United States, Jul. 2018, p. 32, doi: 10.1117/12.2313689.
3. J. Stürmer et al., ‘CARMENES in SPIE 2014. Building a fibre link for CARMENES’, in Advances in Optical and Mechanical Technologies for Telescopes and Instrumentation, Jul. 2014, vol. 9151, p. 915152, doi: 10.1117/12.2056541.
4. Avila, G., “Results on fibre Characterization at ESO,” in [fibre Optics in Astronomy III], Arribas, S., Mediavilla, E., and Watson, F., eds., Astronomical Society of the Pacific Conference Series 152, 44–+ (1998).
5. Murphy, J. D., MacQueen, P. J., Hill, G. J., Grupp, F., Kelz, A., Palunas, P., Roth, M., and Fry, A. (2008). Focal ratio degradation and transmission in VIRUS-P optical bers. In Society of Photo-Optical Instrumentation Engineers (SPIE) Conference Series, volume 7018 of Society of Photo-Optical Instrumentation Engineers (SPIE) Conference Series
6. Sutherland, Adam P.; Stuermer, Julian; Miller, Katrina R.; Seifahrt, Andreas; Bean, Jacob L. Characterizing octagonal and rectangular fibres for MAROON-X. Proceedings of the SPIE, Volume 9912, id. 99125C 10 pp. (2016)
7. G. Avila, B. Buzzoni, M. Casse. fibre characterization and compact scramblers at ESO. Proc. SPIE. 3355, Optical Astronomical Instrumentation.
8. G. Avila, D. Kohler, E. Araya, A. Gilliotte, W. Eckert. Performances of HARPS and FEROS fibres in La Silla ESO Observatory. Proc. SPIE. 5492, Ground-based Instrumentation for Astronomy.
9. <https://spectroscopy.wordpress.com/2009/05/22/slitpinhole-flux-calculator/>